

# A self-powered piezotronic strain sensor based on single ZnSnO<sub>3</sub> microbelts†

Cite this: DOI: 10.1039/c3ra45027a

Jyh Ming Wu,<sup>\*a</sup> Kuan-Hsueh Chen,<sup>b</sup> Yan Zhang<sup>c</sup> and Zhong Lin Wang<sup>\*cd</sup>

We demonstrated a flexible self-powered system that consists of a strain sensor and a nanogenerator. An individual ZnSnO<sub>3</sub> microbelt was bonded at its ends to a polyethylene terephthalate (PET) substrate to fabricate a strain sensor and a single-nanobelt nanogenerator. The sensor and nanogenerator were connected in series and packaged by a polydimethylsiloxane (PDMS) layer. The ZnSnO<sub>3</sub> belongs to a R3C point group that exhibited a large piezopotential along the z-axis, so that it can be either a power source or a sensor. The piezopotential can drive electrons to flow in the circuit and serve as a power source. The piezopotential can also tune the Schottky barrier height (SBH) at the contact by varying the tensile and compressive strain owing to the piezotronic effect, so that it can serve as a strain sensor. The output current decreased as compressive strain increased, but the current increased as tensile strain increased. The sensor can be switched by bending the flexible substrate, which can act as a highly effective reversible electromechanical switcher.

Received 11th September 2013

Accepted 16th October 2013

DOI: 10.1039/c3ra45027a

[www.rsc.org/advances](http://www.rsc.org/advances)

## 1. Introduction

The purpose of a self-powered nanotechnology device is to harvest energy in a living environment to drive a low-power consumption device.<sup>1,2</sup> A self-powered nanosystem<sup>3</sup> should involve not only functional nano-devices but also nanoscale power sources.<sup>4,5</sup> Today, mobile technologies, especially personal and mobile electronics, are becoming very popular. Such devices are widespread and usually consume low amounts of power; however, the production and disposal of current designs can produce non-recyclable garbage that contains toxic heavy metals such as lead. Such electronic waste can be reduced by adoption of miniaturized energy-harvesting, self-powered systems. Lead-free electronic materials are a topic of intense interest. Recently, many authors have reported that perovskite structures such as Pb(Zr,Ti)O<sub>3</sub>,<sup>6</sup> BaTiO<sub>3</sub>,<sup>7,8</sup> NaNbO<sub>3</sub>,<sup>9</sup> and ZnSnO<sub>3</sub> (ref. 10) can be utilized in piezoelectric applications for flexible nanogenerators (NGs) using ferroelectric nanowires/microwires.<sup>11</sup> Our previous works<sup>12</sup> have reported on a promising lead-free ZnSnO<sub>3</sub> material that exhibits a unique non-centrosymmetric (NCS) structure due to its spontaneous

polarization properties. This ZnSnO<sub>3</sub> material demonstrates great potential for piezotronic applications.<sup>10,13</sup>

This work demonstrates a piezotronic strain sensor and a nanogenerator as a self-powered system. The device was made from two single-belts strips of ZnSnO<sub>3</sub> that were separately bonded at the ends on a polyethylene terephthalate (PET) substrate. Due to a spontaneous polarization that is generated along the z-axis in ZnSnO<sub>3</sub> nanobelts/microbelts, the Schottky barrier heights at the semiconductor-metal interfaces can be finely tuned by controlled strain in order to change the inner piezoelectric polarization charges at the interface.<sup>14</sup> The experimental results show that the Schottky barrier height (SBH) of the ZnSnO<sub>3</sub> single-belt structures can be significantly modulated by varied tensile and compressive strains along the z-axis. Our electrical characterization showed that the sensor's response current decreased as compressive strain increased but current increased as tensile strain increased. The work mechanism relies on the piezopotential induced by asymmetrically modulated Schottky barrier height (SBH). Strain can induce a change of internal field, thus the piezopotential can effectively tune the local contact of the metal semiconductor; subsequently the charge carrier transport process can effectively modulate the heights of the Schottky barriers at M-S contacts.<sup>15</sup>

The as-prepared single-belt ZnSnO<sub>3</sub> nanogenerator exhibited an output voltage and current of approximately 0.16 V and 3 nA, respectively. In addition, the self-powered system detected small varied strains from ±0.022% ~ ±0.2%. Tensile strain was denoted as a positive number and compressive strain was denoted as a negative number. This is a first demonstration of a self-powered, ZnSnO<sub>3</sub> based sensor system.

<sup>a</sup>Department of Materials Science and Engineering, National Tsing Hua University, 101, Section 2 Kuang Fu Road, Hsinchu 300, Taiwan. E-mail: wujm@mx.nthu.edu.tw

<sup>b</sup>Department of Materials Science and Engineering, Feng-Chia University, Taiwan

<sup>c</sup>School of Materials Science and Engineering, Georgia Institute of Technology, Atlanta, Georgia 30332-0245, USA. E-mail: zlwang@gatech.edu

<sup>d</sup>Beijing Institute of Nanoenergy and Nanosystems, Chinese Academy of Sciences, China

† Electronic supplementary information (ESI) available: Fig. S1–S3 This material is available in the online version of this article. See DOI: 10.1039/c3ra45027a

## 2. Experimental

The material's synthesis process and devices' fabrication process were reported previously.<sup>10,12</sup> An individual ZnSnO<sub>3</sub> microbelt was carefully bonded at its ends on a polyethylene terephthalate PET substrate; once bonded, it was able to function as either a nanogenerator or a strain sensor. An additional layer of polydimethylsiloxane (PDMS) was used to cover the ZnSnO<sub>3</sub> microbelt to enclose the nanogenerator and strain sensor. This enclosure kept the devices functional under mechanical deformation, as shown by the digital photographic image inset in Fig. 1(a). For electrical measurement, the output voltage and current of the system were measured by a low-noise voltage preamplifier (Stanford Research System Model SR560) and a low-noise current preamplifier (Stanford Research System Model SR570).

## 3. Results and discussions

Fig. 1(a) shows an FESEM images of as-synthesized nanobelts/microbelts that measure  $\sim 10 \times 20 \times 500\text{--}1000 \mu\text{m}$  in thickness, width, and length (see ESI in Fig. S1†). Fig. 1(b) shows an atomic model of the noncentrosymmetric structure that gives rise of piezoelectricity in ZnSnO<sub>3</sub>. The R3C rhombohedral ZnSnO<sub>3</sub> consists of two octahedral cells of ZnO<sub>6</sub> and SnO<sub>6</sub>. The z-axis deviation of Sn and Zn atoms from the octahedral center creates spontaneous polarization. These fundamental semiconductor-piezoelectric coupled properties of ZnSnO<sub>3</sub> enable piezotronics applications such as nanogenerators and strain sensors.<sup>10,12</sup> Fig. 1(c) shows a schematic diagram of a system that consists of a nanogenerator and strain sensor, both of which are made from single-belt ZnSnO<sub>3</sub>. We ignored the free carrier effect to determine the output piezopotential distribution in ZnSnO<sub>3</sub> microbelts. The elastic constants and piezoelectric stress

constants of ZnSnO<sub>3</sub> were used for the theoretical calculations using a Comsol software package.<sup>17</sup> The piezoelectric stress constants,  $e_{11}$ ,  $e_{15}$ ,  $e_{31}$ , and  $e_{33}$  were 0.15, 0.26, 1.23, and 0.29 in  $\text{C m}^{-2}$ , respectively.<sup>18</sup> The elastic constants,  $C_{11}$ ,  $C_{12}$ ,  $C_{13}$ ,  $C_{15}$ ,  $C_{33}$ ,  $C_{44}$ , and  $C_{66}$  were 194, 63, 101, 0.1, 169, 117, and 92 in GPa, respectively.<sup>18</sup> Our theoretical calculations envisioned a compressive strain along the z-axis. The output piezopotential distribution is  $\sim +59 \text{ V}$  (depended on size of the microbelt), as given by Fig. 1(d). The theoretical calculations suggested that the single-belt ZnSnO<sub>3</sub> possesses an excellent piezoelectric response in the application of piezotronic devices.<sup>19</sup>

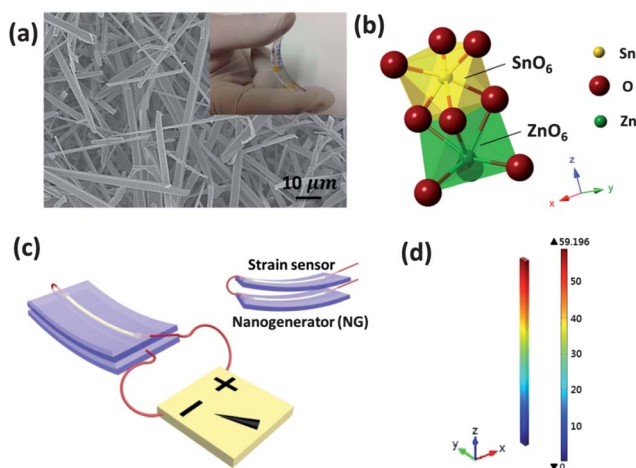
### 3.1 Characteristic strain sensor and nanogenerator

Fig. 2(a) shows  $I$ - $V$  characteristics of the strain sensor under varied compressive and tensile strains that range from  $\pm 0.16$  to  $\pm 0.32\%$ . Fig. 2(a) shows the sensor's rectifying  $I$ - $V$  behavior. The response current of the sensor increased as tensile strain increased but the sensor's response current decreased as the compressive strain increased. As the strains were released, the  $I$ - $V$  curves fully recovered to the origin state.<sup>12,16</sup> Based on the experimental results, we suggest that thermionic emission-diffusion phenomena (see eqn (1) in ESI†) governed these sensor devices. Regarding the approximation of the thermionic emission-diffusion equation, Fig. S2† shows that the  $\ln I$ - $V^{1/4}$  curve is almost linear. The Schottky barrier formula can be explained by our experimental data. Therefore, we can use the model of strain-induced change in the SBH of the ZnSnO<sub>3</sub> to explain how the sensitivity of the SBH changes as a function of varied strain.<sup>20</sup> By means of the Saint-Venant bending theory,<sup>20,21</sup> the compressive and tensile strains were therefore estimated as 0,  $\pm 0.16\%$ , and  $\pm 0.32\%$ .

Under a reverse bias of  $-0.6 \text{ V}$ , the change of SBH ( $\Delta\Phi_{\text{B}}$ ) with strain was calculated and the data were plotted in Fig. 2(b). The change of SBH showed a linear relationship. Fig. 2(b) shows that the SBH increased as the compressive strain increased and the SBH decreased as the tensile strain increased. The strain modified the semiconductor's band gap and therefore the piezoelectric polarization exhibited a linear relationship with strain.<sup>22,23</sup> This demonstrates that the SBH of the ZnSnO<sub>3</sub> microbelt can be significantly modulated by application of compressive and tensile strain.

The current response of the strain sensor was evaluated over many repeated cycles of tensile and compressive strain at a frequency at a fixed bias of  $2 \text{ V}$ . Response current was increased by increase of tensile strain and decreased by the release of tensile strain (see Fig. 2(c)). In contrast, the response current was decreased by increase of compressive strain and increased by the release of compressive strain (see Fig. 2(d)). The tensile and compressive strains can be switched by bending the flexible substrate. The strain sensor can be used as an effective electromechanical switch and the change is highly reversible at a constant bias of  $\sim 2 \text{ V}$ . This is consistent with our results as given by Fig. 2(a).

In order to illustrate the strain-induced piezopotential that affected the SBH at source and drain contacts, schematic band diagrams of Figures 3(a)–(d) were devised for the piezotronic



**Fig. 1** (a) FESEM image of ZnSnO<sub>3</sub> microbelts. Inset image is a digital micrograph of the nanogenerator/strain sensor. (b) Atomic model of the rhombohedral structure ZnSnO<sub>3</sub>. (c) The schematic diagram of the self-powered strain-sensing system made from a nanogenerator and strain sensor. (d) Theoretical calculation of the piezoelectric potential distribution in a ZnSnO<sub>3</sub> microbelt under an axial compressive stress.

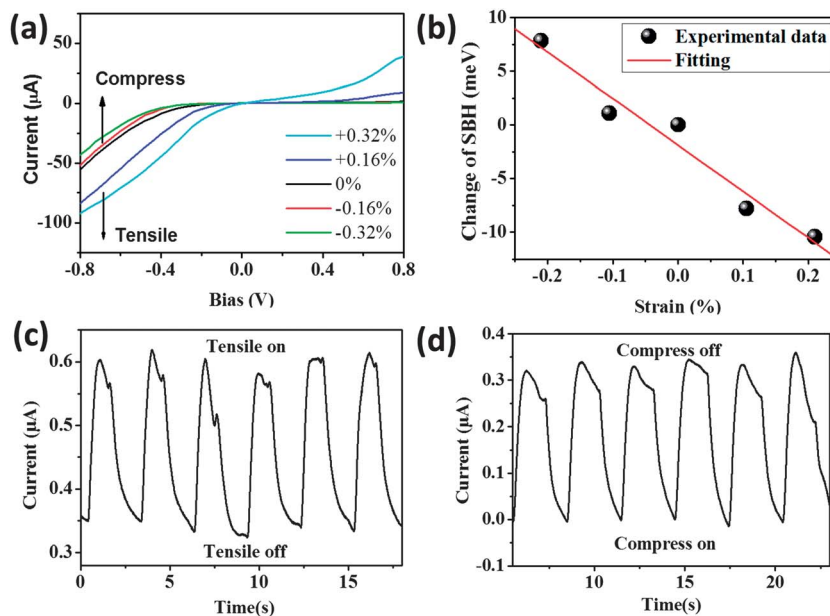


**Fig. 2** (a)  $I$ - $V$  characteristic of a strain sensor under varied compressive and tensile strains. (b) By utilizing the thermionic emission-diffusion model to estimate the change in SBH as a function of varied strain. (c) Current response of a strain sensor that was repeatedly by a tensile and (d) compressed stress.

effects<sup>24</sup> in the  $\text{ZnSnO}_3$  microbelts. On the basis of the  $I$ - $V$  characteristics, we assume that the structure of the strain sensor can be regarded as back-to-back with Schottky barrier heights (SBHs) of  $\Phi_s$  and  $\Phi_d$  (in eV), as shown in Fig. 3(a). When the sensor was in a strain-free (unstrained) state, the SBH was measured at the source (e.g.,  $\Phi_d$ ) and drain contact (e.g.,  $\Phi_s$ ) (see Fig. 3(b)). Fig. 3(c) and (d) illustrate how the strain influenced the piezopotentials of the sensor at the source and drain contacts. As the sensor was subjected to tensile strain, a higher piezoelectric potential ( $V_{p+}$ ) appeared at the drain contact while

a lower piezoelectric potential ( $V_{p-}$ ) formed at the source contact; thus the SBH at the source contact became higher and the SBH at the drain contact became lower (see Fig. 3(c)). By contrast, as the tensile strain was switched to a compressive strain, a higher piezopotential ( $V_{p+}$ ) appeared at the source side while a lower piezoelectric potential ( $V_{p-}$ ) appeared at the drain side, thus producing a higher SBH at the drain side and a lower SBH at the source side (see Fig. 3(d)). Thus, by applying an external strain to the sensor, the internal piezopotential field can be changed and the local contact characteristics can be

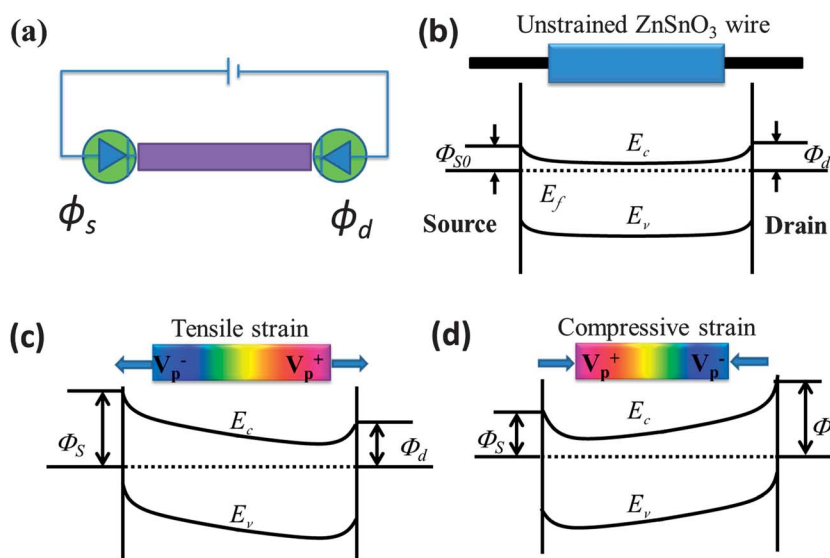


**Fig. 3** Energy band diagram presents the asymmetric SBH at the source and drain contacts of a single-belt  $\text{ZnSnO}_3$  (a) A back-to-back with SBH of a sensor made from  $\text{ZnSnO}_3$ , which is subjected to (b) no strain, (c) tensile strain, and (d) compressive strain. These illustrate the piezopotential of the microbelt can be finely tuned by varied strains.

modulated. The characteristic piezopotential depended on the crystallographic orientation of the nanobelt/microbelt and the variety of strain.<sup>25</sup>

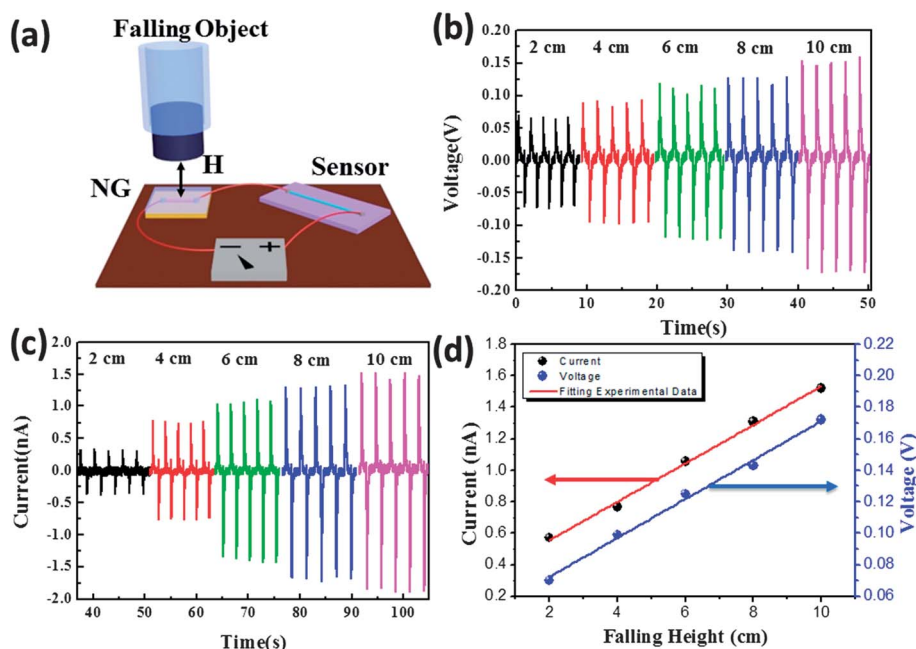
A single-belt strip of ZnSnO<sub>3</sub> was used as a nanogenerator; this was evaluated by low noise voltage and a current preamplifier. The schematic diagram of Fig. 4(a) shows the different degrees of impact. The nanogenerator was placed on a stage to test a collision by a free-falling object with the frequency of 0.33 Hz. Results showed that various amounts of momentum in the falling object produced various corresponding output voltages and currents. The object was dropped from heights of 2, 4, 6, 8, 10 cm; the object weighed 300 g. The corresponding output voltages and currents are shown in Fig. 4(b) and (c), respectively. The output voltage and current were proportional to object's initial height, as shown in Fig. 4(d). Therefore, the collision momentum is proportional to the varied height.<sup>26</sup>

Fig. 5(a)–(b) demonstrates that a nanogenerator can produce a maximum output voltage and current of  $\sim 0.16$  V and 3 nA, respectively. The working mechanism can be explained as follows. When the nanogenerator was subjected to a compressive strain, it generated a piezopotential on one of the contact sides (*i.e.*, the drain-contact) and raised its Fermi-level, causing electrons to flow from the drain-contact to the source-contact through the external load to generate the output voltage and current. The Schottky barrier height at the source-contact therefore blocks the electrons' flow into the microbelt so that the electrons tended to accumulate at the interface region of the semiconductor microbelt at source contact until the potentials were balanced at both sides of the electrodes. As the strain was released in the nanogenerator, the disappearance of the piezopotential caused a lower Fermi level at the drain-contact. The

accumulated electrons at the source-contact were returned from the source to the drain-contact through the external load to balance the potential; thus the nanogenerator returned to its original state, which generated negative output voltage and current.

### 3.2 Self-powered sensor system

Two strips of single-belt ZnSnO<sub>3</sub> were separately bonded at their ends on a flexible substrate. These two strips served as a strain sensor and nanogenerator; they were enclosed to enhance their robustness as a self-powered strain-sensing system. This strain sensor can be regarded as a variable resistor, as shown in the schematic diagram of the equivalent circuit in the upper inset image of Fig. 5(c). As the self-powered strain-sensing system was subjected to a tensile strain, the nanogenerator periodically produced a peak voltage to the strain sensor. Since the sensor decreased its resistance as the tensile strain increased, the corresponding output current of the system was increased (see Fig. 5(c)). In contrast, as the system on a common substrate was subjected to a compressive strain (see the schematic diagram in the inset of Fig. 5(d)). The corresponding output current decreased as the compressive strain increased (see Fig. 5(d)). This is consistent with our sensor's characteristic *I*-*V* curves (see Fig. 2(a)). The sensor's resistance decreased as its tensile strain increased, but resistance increased as its compressive strain increased. We have measured a series sample of our sensors' resistance, which is in the range of  $10^8$  to  $10^{10}$   $\Omega$ . In this work, the sensor' inner resistance is  $\sim 2.31 \times 10^8$   $\Omega$ , which is around two order lower than that of nanogenerator ( $3.45 \times 10^{10}$   $\Omega$ ) (see ESI of Fig. S3†). Therefore, we



**Fig. 4** (a) Schematic diagram of the nanogenerator testing method. (b and c) The output voltage and current of the nanogenerator under impact (0.33 Hz) exerted by a free-falling object with different heights of 2, 4, 6, 8, and 10 cm; the object weighed 300 g. (d) The output voltage and current as function of varied height; experimental and fitting curves.

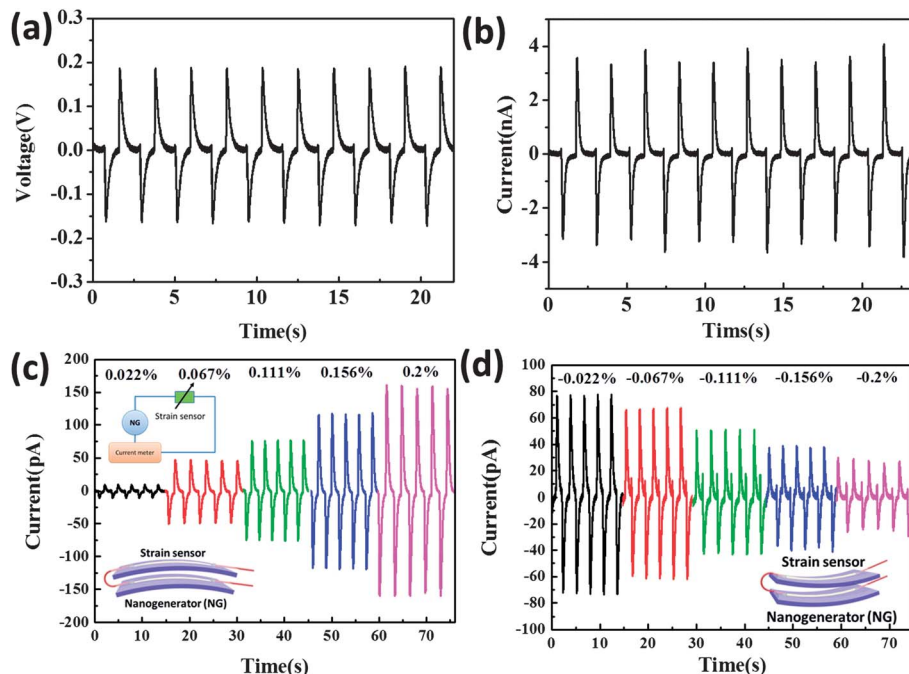


**Fig. 5** (a) and (b) The electrical output voltage and current result from a nanogenerator. (c) The corresponding output current of the self-powered strain-sensing system as subjected by tensile strain (lower inset is the schematic diagram of system by application of tensile strain and equivalent circuit, upper inset), and (d) output current of the self-powered strain-sensing system as subjected by compressive strain (inset is the schematic diagram of the system by application of compressive strain).

suggest that such resistances still can provide a slightly internal conduction through the nanobelt as for the sensor, namely, the current can flow through the sensor but not the nanogenerator. This is a simple demonstration that our nanogenerator and strain sensor can be integrated into a self-powered system. It is highly likely that such a device could be useful for human-computer interfaces and smart sensor systems.

## 4. Conclusions

In summary,  $\text{ZnSnO}_3$  microbelts were formed into a flexible strain sensor and nanogenerator that were integrated to form a self-powered strain-sensing system, which included an energy-harvesting and finely-tuned piezotronic system. The nanogenerator can produce a voltage and current of 0.16 V and 3 nA, respectively. The system was able to self-powered detect strains that ranged from  $\pm 0.022 \sim \pm 0.2\%$ . When the system was subjected to a compressive strain, the corresponding output current of the system decreased as the compressive strain increased. In contrast, the corresponding output current of the system increased as the tensile strain increased. The strain can effectively modulate the height of the microbelt's SBH, which allowed the device's electron transport properties to be finely tuned.

## Acknowledgements

The authors would like to thank the National Science Council of the Republic of China for financially supporting this research

under Contract number NSC: 100-2628-E-035-006-MY2; NSC 102-2221-E-035-019-MY3.

## References

- 1 P. X. Gao, J. H. Song, J. Liu and Z. L. Wang, *Adv. Mater.*, 2007, **19**, 67; Y. Qin, X. D. Wang and Z. L. Wang, *Nature*, 2008, **451**, 809–813.
- 2 Z. L. Wang, *Adv. Mater.*, 2012, **24**, 280–285.
- 3 Z. L. Wang and J. H. Song, *Science*, 2006, **312**, 242–246.
- 4 X. D. Wang, J. H. Song, J. Liu and Z. L. Wang, *Science*, 2007, **316**, 102–105.
- 5 X. D. Wang, J. H. Song, J. Liu and Z. L. Wang, *Science*, 2007, **316**, 102–105.
- 6 S. Xu, B. J. Hansen and Z. L. Wang, *Nat. Commun.*, 2010, **1**, 93–97.
- 7 K. I. Park, S. Xu, Y. Liu, G. T. Hwang, S. J. L. Kang, Z. L. Wang and K. J. Lee, *Nano Lett.*, 2010, **10**, 4939–4943.
- 8 Z. H. Lin, Y. Yang, J. M. Wu, Y. Liu, F. Zhang and Z. L. Wang, *J. Phys. Chem. Lett.*, 2012, **3**, 3599–3604.
- 9 J. H. Jung, M. Lee, J. I. Hong, Y. Ding, C. Y. Chen, L. J. Chou and Z. L. Wang, *ACS Nano*, 2011, **5**, 10041–10046.
- 10 J. M. Wu, C. Xu, Y. Zhang and Z. L. Wang, *ACS Nano*, 2012, **6**, 4335–4340.
- 11 J. M. Wu, C. Xu, Y. Zhang, Y. Yang, Y. Zhou and Z. L. Wang, *Adv Mater.*, 2012, **24**, 6.
- 12 J. M. Wu, C. Y. Chen, Y. Zhang, K. H. Chen, Y. Yang, Y. F. Hu, J. H. He and Z. L. Wang, *ACS Nano*, 2012, **6**, 4369–4374.
- 13 K. K. Shung, J. M. Cannata and Q. F. Zhou, *J. Electroceram.*, 2007, **19**, 141–147.

- 14 S. A. P. Stoyanov and J. M. White, *Surf. Interface Anal.*, 1990, **15**, 7.
- 15 Z. L. Wang, *Nano Today*, 2010, **5**, 540–552.
- 16 J. Zhou, P. Fei, Y. Gu, W. Mai, Y. Gao, R. Yang, G. Bao and Z. L. Wang, *Nano Lett.*, 2008, **8**, 3973–3977.
- 17 Comsol Model Gallery (Semiconductor Diode).
- 18 J. Zhang, B. Xu, Z. Qin, X. F. Li and K. L. Yao, *J. Alloys Compd.*, 2012, **514**, 113–119.
- 19 Y. Zhang, Y. Liu and Z. L. Wang, *Adv Mater.*, 2011, **23**, 3004–3013.
- 20 J. Zhou, Y. D. Gu, P. Fei, W. J. Mai, Y. F. Gao, R. S. Yang, G. Bao and Z. L. Wang, *Nano Lett.*, 2008, **8**, 3035–3040.
- 21 Y. Inaguma, M. Yoshida and T. Katsumata, *J. Am. Chem. Soc.*, 2008, **130**, 6704–6705.
- 22 E. D. Minot, Y. Yaish, V. Sazonova, J. Y. Park, M. Brink and P. L. McEuen, *Phys. Rev. Lett.*, 2003, **90**, 156401.
- 23 J. Cao, Q. Wang and H. Dai, *Phys. Rev. Lett.*, 2003, **90**, 157601.
- 24 Z. L. Wang, *J. Phys. Chem. Lett.*, 2010, **1**, 1388–1393.
- 25 R. M. Yu, L. Dong, C. F. Pan, S. M. Niu, H. F. Liu, W. Liu, S. Chua, D. Z. Chi and Z. L. Wang, *Adv. Mater.*, 2012, **24**, 3532–3537.
- 26 L. Gu, N. Cui, L. Cheng, Q. Xu, S. Bai, M. Yuan, W. Wu, J. Liu, Y. Zhao, F. Ma, Y. Qin and Z. L. Wang, *Nano Lett.*, 2013, **13**, 91–94.